12-13-2002

Effects of Brain Region and Gender on Proton Magnetic Resonance Spectroscopy in Normal Subjects

Marlyanne Pol-Rodriguez

Effects of Brain Region and Gender on Proton Magnetic Resonance Spectroscopy in Normal Subjects.

A Thesis Submitted to the
Yale University School of Medicine
in Partial Fulfillment of the Requirements for the
Degree of Doctor of Medicine

by

Marlyanne M. Pol-Rodriguez

2002

EFFECTS OF BRAIN REGION AND GENDER ON PROTON MAGNETIC RESONANCE SPECTROSCOPY IN NORMAL SUBJECTS.

Marlyanne M. Pol-Rodriguez and Robert K. Fulbright. Section of Neuroradiology, Department of Diagnostic Radiology, Yale University School of Medicine, New Haven, CT.

The purpose of this study was to acquire spectra using proton magnetic resonance spectroscopy (MRS) with a long echo time (TE) to measure clinically important brain metabolites in normal subjects. We aimed to determine whether these metabolites vary across brain regions and between men and women. The results of this study will constitute a normative database that will be used as a reference for MRS studies of patients with neurological disease.

Single voxel proton (^{1}H) spectra were acquired in seventy-two subjects ranging in age from twenty to forty-four years. Ten brain regions were examined. Six gray matter sites in the cerebrum included four cortical areas in the frontal, parietal, temporal, and occipital lobes, and two deep nuclear sites in the basal ganglia and the thalamus. Two cortical white matter regions were in the parietal and the frontal lobes. Two posterior fossa sites included the pons and the cerebellum. For each spectrum, the metabolites N-acetyl aspartate (NAA), creatine (Cr) and choline (Ch) were identified. Ratios of NAA/Cr and Ch/Cr were calculated for each brain region. A multifactorial analysis of variance was performed with the two metabolic ratios as dependent variables and with brain region and gender as independent variables. Post-hoc statistical analysis consisted of the Scheffé's F statistic for significant difference between pairs of brain regions for both metabolic ratios.

There was significant regional variation for both the NAA/Cr ratio ($p < .0001$) and the Ch/Cr ratio ($p < .0001$). The NAA/Cr ratio was consistent within cortical gray and white matter but differed between cortical gray (smaller ratio) and white matter (larger ratio). The Ch/Cr ratio was variable in the gray matter, differed between some but not all gray and white matter regions, but was consistent within cortical white matter regions. There was no difference between men and women for either metabolic ratio. These findings provide the requisite normative values to use single voxel, long TE MRS in adult patients with neurological disorders.

ACKNOWLEDGEMENTS

The authors thank the MR technicians at the Yale School of Medicine MRI Center, especially Terri Hickey, Hedy Sarofin, and Cheryl McMurray for their technical assistance in this project. The authors also thank all the subjects who volunteered their time to participate in this study. Completion of this thesis was partly supported by short-term research funding from the Office of Student Research at Yale University School of Medicine.

TABLE OF CONTENTS

INTRODUCTION

The phenomenon of nuclear magnetic resonance (MR) originates from the interaction between atomic nuclei and an external magnetic field. The property of the nucleus necessary for MR is the nuclear spin or spin angular momentum, which can be described using both classical physics and quantum mechanics. The classical physics approach explains the interaction between the external magnetic field and a nucleus that has spin angular momentum. A quantum mechanical treatment is necessary to obtain information about the interaction of electromagnetic waves and nuclear spins. The quantum mechanical description dictates that the nuclear spin has quantized, discrete values that depend on the specific nature of the nucleus. Nuclei with even atomic weights and atomic numbers have a spin of zero (or no spin). Nuclei with an even atomic weight and an odd atomic number have a whole number spin. Nuclei with odd atomic weights have a half integer spin, the most common class seen in clinical spectroscopy (1). Most nuclei studied in biological systems using MR techniques have a spin of ½. Due to the low sensitivity of instrumentation, individual nuclei are not examined in the MR experiment; instead, the entire collection of nuclei, or spins, inside a volume of interest is treated as a unit because a larger entity is easiest to study. The number of nuclei present per volume of tissue depends on the specific nucleus being examined.

If a tissue is placed inside a magnetic field, individual spins begin to rotate about the magnetic field at a frequency proportional to the applied magnetic field and the gyromagnetic ratio, which is characteristic for a specific nucleus. These nuclei will distribute themselves between different energy levels depending on the spin quantum number. The interaction of a spin with the external magnetic field produces a coupling

between the spin and the magnetic field that causes the spin vector component parallel to the magnetic field to begin to have discrete values. For a spin of ½, the only possible values for such spin component are + ½ (parallel spin) and – ½ (antiparallel spin). The parallel component is lowest in energy and the antiparallel component is highest in energy. In the presence of a magnetic field, the tissue will have a slight excess of spins in the lower energy state, compared to the higher energy state. In other words, the tissue will be magnetized (1).

The difference in energy between two adjacent spin states is proportional to the strength of the applied magnetic field. As the magnetic field strength increases, the intensity of the MR signal increases because the energy separation between the spin states increases, and because more nuclei in the lower energy state can now be excited to the higher energy state (2). When an electromagnetic pulse equal to this energy difference is applied to a magnetized tissue, a spin in the lower energy state will be excited to the higher energy state. This process is called resonance absorption. Because there are more spins in the lower energy state, the tissue will experience a net absorption of energy. Following excitation with an electromagnetic pulse in the radiofrequency range, the spins will reemit the absorbed energy at the same frequency and return to the lower energy level through a process called relaxation (1).

The resonance phenomenon of MR is achieved by applying an oscillating magnetic field (a radiofrequency pulse) perpendicular to the vector of the angular momentum. The radiofrequency pulse (rf) has the same frequency as the Larmor frequency. Following the excitation pulse, the spins are flipped into the horizontal, or *xy* plane. The spins will then decay or return to their original equilibrium orientation. The

proportion of magnetization that is perpendicular to the external magnetic field will induce a voltage in a receiver coil. The voltage generated in the receiver coil is the MR signal and is known as the free induction decay (1). The free induction decay is a time domain signal that consists of the superposition of several signals that evolve at different frequencies and decay with different time constants. This time domain signal is converted from a function of time to a function of frequency using the Fourier transformation, and the MR spectrum is produced. The spectrum is a display of absorption peaks occurring at the various frequencies that contribute to the entire signal. The position, amplitude, and width of each peak depend on the frequency, amplitude, and decay time of the corresponding components. The integrated peak area is proportional to the number of spins creating the signal. The peak position serves to identify the kind of spin examined, and its distinct molecular environment.

Chemical compounds containing a particular nucleus can have slightly different resonance frequencies than those predicted for the nucleus alone due to the interactions of the negatively charged electrons that surround the nucleus. Electrons have spin properties similar to the protons and neutrons in the nucleus of the atom. When placed in an externally applied magnetic field, electrons precess and generate a small magnetic field around the nucleus. These local magnetic fields created by the electrons can add or subtract strength from the external field. As a result, the nucleus experiences a slightly altered magnetic field, and resonates at a slightly shifted frequency (2). This phenomenon is called chemical shift and is one of the important properties of MR spectroscopy. The chemical shift determines the resonance frequency position of each peak on a MR spectrum. Chemical shift can be expressed as an absolute frequency, which is dependent

on magnetic field strength. It can also be expressed as parts per million from the main magnetic resonance frequency of the system used, which is independent of the strength of the magnetic field (3).

Relaxation is another important concept in MR. Relaxation is described as the process by which spins return to equilibrium after an initial perturbation (excitation). Relaxation times differ between tissue types, and this difference is mainly responsible for the contrast seen in conventional MR Images. Relaxation time measurements are incorporated in the quantitative analysis of MR spectra to obtain tissue metabolite concentrations and to gain insight into the molecular environments of spins. Relaxation time differences between nuclei can also be used to selectively suppress signals to simplify spectra. Two measures of relaxation are well defined, both of which describe energy transfer by the excited spin. The relaxation time T1, known as the spin-lattice relaxation time or longitudinal relaxation time, represents the restoration of the longitudinal equilibrium. It is the time necessary for the *z* component of the magnetization to return to 63% of its initial value after an excitation pulse (1). In clinical MR spectroscopic (MRS) measurements, the magnetization achieves a steady state because multiple radiofrequency pulses are applied repeatedly, and the time between excitation pulses, TR, is almost never enough for complete return to equilibrium. In T1 relaxation, the energy absorbed after each pulse is transferred from the excited spin to its surroundings. Most metabolites that are studied using MR spectroscopy have relatively long T1 relaxation times, therefore, short TR times will result in significantly saturated spins which makes quantification of signals difficult.

T2 relaxation, also known as spin-spin relaxation or transverse relaxation, represents the restoration of the transverse magnetization. It is the time it takes the transverse component of the magnetization to decay to 37% of its original value. At equilibrium (prior to excitation), the net magnetization is oriented along the *z* axis of the applied magnetic field. After a 90° radiofrequency pulse, the longitudinal magnetization disappears because the net magnetization rotates into the *xy* plane, so that at the end of the pulse, the coherence or uniformity of the spins is in the transverse plane. Each spin is synchronized and precesses at the same frequency such that a nearby spin of the same kind will experience the same molecular environment and will easily absorb the energy that is released. T2 relaxation refers to the energy relocation from an excited spin to a nearby synchronized spin (1).

After energy absorption by the spins in a tissue, intermolecular and intramolecular interactions, like vibrations or rotations, will cause the magnetic field around each spin to fluctuate, inducing variations in their precessional frequency. This local field fluctuation causes a gradual, irreversible loss of phase coherence as the spins exchange their energy and the total transverse magnetization decreases. The modulation of the spin's local magnetic field due to vibrations and rotations is responsible for spin-spin relaxation. T2 relaxation can often be used to measure the restriction of molecular motion of a spin: the longer the T2 relaxation, the more free or random the spin movement. With the passage of time, the transverse coherence completely disappears and reforms in the longitudinal direction through the process of T1 relaxation (1). Another reason for the loss of transverse phase coherence is the inhomogeneity of the magnetic field. A spin always experiences a fluctuating local magnetic field which causes changes in its precession

frequency and lead to a loss in transverse phase coherence. When a dephased spin in the transverse plane experiences a 180° radiofrequency pulse, it will in effect reverse its phase relative to the resonant frequency, without changing its rate and direction of precession. After a short delay of time, the spin will regain its transverse coherence. Regaining of phase coherence induces a spin echo, a voltage in the receiver coil (1). Echo time (TE) is the time between the excitation pulse and the 180° radiofrequency pulse in a spin echo experiment.

Nuclei within a molecule can interact and affect the local magnetic field around each other, an effect known as spin coupling. In a magnetic resonance spectroscopy (MRS) measurement, the choice of echo time, TE, complicates the spectrum if the spins under observation are coupled. Coupled spins preserve their frequency difference in spite of any radiofrequency pulse or the static magnetic field. As a result, the phase modulation of the signal is dependent on the time between radiofrequency pulses (1). Changing the TE changes the type of information that can be obtained. Using a short TE (< 30 ms) allows observation of metabolites with short relaxation times along with metabolites that show up at longer TE. The shortest possible TE produces the smallest losses secondary to T2 relaxation and therefore the best signal-to-noise-ratio (SNR). Conversely, the background signals from short T2 components are significantly larger at short TE, and also, shorter and less specific radiofrequency pulses have to be used, potentially leading to more signal contamination from outside the volume of interest (4). Short TE affects not only the appearance of the peak, but also the intensities of the peaks because each metabolite has its own relaxation time. Using long TE, only the signals from choline (Ch), creatine (Cr), N-acetyl aspartate (NAA), and lactate are detected. The use of short

TE, on the other hand, allows for identification of other metabolites like myoinositol, glutamate, glutamine and glycine (3).

It is important to have the best possible magnetic field homogeneity over the volume of interest for MRS analysis. Good field homogeneity allows the resolution of resonances with frequencies that are close together. Most MR systems use a set of coils known as shim coils to compensate for field distortions due to manufacturing imperfections or environmental interference. Shimming is a procedure for optimizing the field homogeneity, globally and locally, over the selected volume of interest. Uniform magnetic field homogeneity leads to better spectral peak resolution and also decreases the time required to obtain spectral information because of improved SNR (1;2).

The robust signal from the inherently high MR sensitivity of protons and the large water content of biological tissue make clinical MR images possible. In MR spectroscopy, however, the large water signal makes it very difficult to detect signals from metabolites that have concentrations 10,000 to 100,000 times smaller than water. Sensitivity is essential in clinical MRS, and measurement sequences must include ways to suppress the prevalent water signal. Suppression does not have to be complete, but at least a 50-100 fold reduction in the water peak amplitude is needed. Reduction of the water signal by at least a factor of 1000 can be accomplished through a method know as chemical shift selective excitation or *CHESS,* which uses low-power frequency selective pulses to saturate the water proton resonance frequency and suppress the signal. The residual water signal can be subtracted from the MR signal after data processing and phase corrections (1-3).

In the clinical application of MR spectroscopy, selected localization techniques allow the definition of small tissue volumes of interest, using anatomical MR images as reference. Localization techniques may be characterized as single volume (or voxel) or multivolume. In single voxel spectroscopy, a spectrum is obtained from a small volume of tissue demarcated by the intersection of three orthogonal planes. There are three main single voxel techniques, but only two of them are commonly employed clinically. Stimulated echo acquisition mode (STEAM) and point resolved spectroscopy (PRESS) techniques employ frequency selective radiofrequency pulses to excite the volume of interest only. The image selective in vivo spectroscopy (ISIS) technique, which is not commonly used clinically, employs generalized excitation and subsequent subtraction (cancellation) of unwanted signals from surrounding tissue outside the volume of interest (1). Both STEAM and PRESS are highly effective volume localization schemes, but there are some major differences between them. The STEAM technique is better for measurements involving short echo times (TE < 20 ms), and also achieves more successful water signal suppression than PRESS, but the STEAM sequence looses signal intensity by a factor of two and is highly susceptible to motion, multiple quantum effects and diffusion processes. PRESS is the volume localization method of choice for long echo times (TE > 135 ms). This sequence also has better signal intensity and is less sensitive to patient motion and quantum effects (1;2).

Multiple voxel spectroscopy can be one-dimensional, two-dimensional, or three-dimensional, and this technique is usually performed using chemical shift imaging (CSI). CSI is a method that employs features of both conventional MR imaging and spectroscopy. It is a technique for collecting in one measurement MR spectra from

multiple contiguous voxels covering a large region of interest. Data is obtained as spectral maps and metabolite images, and these can be superimposed on conventional MR images to compare changes in spectra from adjacent voxels, or to obtain the distributional pattern of a particular metabolite within the tissue segment examined. Although multiple measurements can be obtained at once using this technique, the SNR for those values is much lower than that of single voxel measurements because good shim and uniform water suppression is difficult to achieve over a large, heterogeneous volume (1;2).

Magnetic Resonance Spectroscopy (MRS), a tool that has been used extensively in research, has recently become a useful clinical technique to study the cellular and molecular mechanisms of neuronal activity in the living brain. Proton MRS studies can provide a non-invasive source of information for several brain compounds. *In vivo* MRS studies of the brain can quantify the steady-state levels of neurochemicals, like glutamate (Glu), *N*-acetyl aspartate (NAA) and γ-aminobutyric acid (GABA), which can be used as markers for neuronal density and may reflect functional-synaptic properties, since they are predominantly located within neurons (3;5;6). Other metabolites that can be measured with proton MRS are choline (Ch), which is a chemical found in myelin and cell membranes and is a marker of cell turnover and cell density; creatine and phosphocreatine complex (Cr), markers of the energetic status of neurons; lactate, a product of cell metabolism especially during anaerobic states; and glucose, glutamine, lipids and myoinositol. The normal distribution of these chemicals in the brain has not been studied extensively, but abnormal values have been observed in many neurological diseases.

Long TE spectra (TE = 135 and 270 ms) obtained from proton MRS reveal the major contributors to the proton signal to be NAA, Ch and Cr. The presence of NAA in an MR spectrum can be attributed to its N-acetyl methyl group, which resonates at 2.02 ppm. Other less abundant N-acetyl groups also contribute to this peak. The exact role of NAA in the brain is unknown, but it is believed to be a marker for neurons. NAA has been shown to increase during brain development after birth and in childhood, and to decrease with aging (1;7-10). A decrease in NAA concentration has been documented in diseases involving neuronal and axonal loss, such as epilepsy, stroke, the majority of dementias, hypoxia, encephalopathies, leukodystrophies, tumors, multiple sclerosis, and other white matter diseases (3;6;11-18). Increased NAA is found in children with Canavan's disease, which is a genetic disorder where the enzyme that catabolizes NAA is defective (10).

The peak for Ch occurs at 3.22 ppm. It arises from protons on methyl groups attached to nitrogen in choline and other trimethyl ammonium compounds. Choline is a component of the phospholipid metabolism of cell membranes and reflects membrane turnover, and it is also a precursor for the synthesis of acetylcholine and phosphatidylcholine (3). Increased choline probably suggests increased membrane synthesis or breakdown, and can also indicate increased number of cells. The choline peak in the brain arises primarily from phosphorylcholine and glycerophosphorylcholine. Other compounds such as taurine and phosphoryl-ethanolamine also contribute to the signal at 3.22 ppm. These compounds are particulary high in the immature brain. Choline is the largest peak in normal spectra of neonate brain, and there is a decrease in Ch concentration as the brain matures and develops (1;7;9;10). An increase in the Ch

peak area in the adult brain is associated with Alzheimer's disease, post-liver transplant, primary and secondary brain tumors and epilepsy (1;6;13). A decrease in the Ch peak is seen in hepatic encephalopathy and subacute and chronic cerebral infarction.

The peak for total Cr is seen at 3.03 ppm and it contains major contributions from both creatine and phosphocreatine. Phosphocreatine (PCr) is thought to play a role in sustaining energy-dependent systems in brain cells by functioning as a reservoir for high-energy phosphates and as a buffer in ATP and ADP stores. Cr can increase in hypometablic states and trauma, and decrease in hypermetabolic states, hypoxia, stroke and tumor. Cr has been considered stable enough, even in face of disease, to be used as an intrinsic reference for reporting relative concentrations of other chemicals in the brain, since it measures both Cr and PCr, which are maintained at equilibrium by creatine kinase (1;3)

Lactate, if elevated, is also readily detectable using long TE spectroscopy and appears as a doublet at 1.33 ppm. Lactate levels in the brain are normally low (less than 1 mM) such that it is usually not seen in the spectra of normal brain. The presence of lactate typically indicates that non-oxidative carbohydrate catabolism is happening. Lactate has been detected in patients with stroke, some brain tumors, hypoxia, anoxia, mitochondrial encephalopathies, and in epileptic foci immediately after a seizure (1;3;10;13;14).

Other metabolites that can be studied with MRS in vivo require short TE sequences for visualization. The most prominent of these is myoinositol, a metabolite involved in hormone-sensitive neuroreception when it is phosphorylated. Myoinositol increases in Alzheimer's disease and diabetes mellitus, and decreases in stroke, tumor

and hypoxic encephalopathy. Other signals seen include: glutamine and glutamate; glucose, which is elevated in spectra of diabetic patients; GABA, increased in epileptic patients treated with vigabatrin; and lipid signals, seen in some tumors, stroke and acute MS lesions (1;3).

Several studies have observe regional variations in normal brain metabolites (5;19-21) as well as variations with age (7-9;22). Grachev et al. noted significantly different metabolite concentrations between six regions of the brain, with the highest concentration shifts for the nine metabolites measured happening in the prefrontal regions (5). Michaelis et al. reported great heterogeneity of eight metabolites between brain regions, and found highest NAA concentrations in pons and parietal gray matter, and highest Ch concentrations in pons and cerebellum (19). Kreis et al. found NAA/Cr and Ch/Cr ratios to be higher in parietal white matter when compared to gray matter spectra (20). Komoroski et al. also observed significant regional differences in the major brain metabolites when compared across regions of the brain, and reported a lower NAA/Cr in the hippocampus, and lower NAA/Cr and Ch/Cr in basal ganglia (21). Regarding age, earlier studies have shown that the dominant peak in short TE spectra of human brain changes from being myoinositol in neonates, to Ch in older infants, to NAA in adults. Some studies have shown that metabolite variations in adulthood are marked by decreased NAA, Cr and Ch levels in older adults compared to young adults (23;24).

There is only a relatively small amount of data published addressing the effects of gender on ^{1}H MRS in normal individuals, and the conclusions of these studies have been conflicting. Charles et al., using the STEAM voxel technique (TE = 270 ms) with CSI, saw no gender differences in NAA/Cr, NAA/Ch and Ch/Cr ratios in white matter, and

cortical and noncortical gray matter (24). In contrast, Wilkinson et al., using a PRESS sequence and TE = 135 ms, saw significantly smaller NAA/Ch and larger Ch/Cr ratios in parieto-occipital white matter of males compared to females (25). Pouwels and Frahm saw no gender differences using STEAM localization and TE = 20 ms to quantify metabolite concentrations in several brain regions, except for a 1.3-fold higher myoinositol level in parietal white matter of females. (26). Komoroski et al. again found no difference between genders for the metabolite ratios measured in seven different regions of the brain using STEAM sequence at TE = 30 ms (21). Most recently, Grachev and Apkarian, also using STEAM at TE = 30 ms, demonstrated gender differences due to increased levels of NAA in female sensorimotor cortex, and increased glucose in female orbital frontal cortex (5).

No differences in metabolite concentrations have been reported between equivalent locations in the right and left hemispheres of normal brain, but significant differences in chemical concentrations, including NAA, Cr and myoinositol, have been reported between white and gray matter (5;19-21). The proportion of gray and white matter in a region of interest has the greatest effect on metabolite concentrations and ratios.

STATEMENT OF PURPOSE AND HYPOTHESIS

MRS techniques are very sensitive to minor changes in parameters, and therefore, normal values must be established based on the methods used at each institution. This study used the MRS techniques employed by the clinical MRI center at the Yale University School of Medicine to measure three different brain metabolites: NAA, Ch and Cr. The ratios of NAA/Cr, and Ch/Cr were calculated in ten different brain regions in normal adult males and females. Having normal values of these brain metabolites, which can be used as a reference in the clinical application of MRS, will advance the ability to use MRS to diagnose patients with neurological diseases.

We had three basic hypotheses for the age range of adults in our study: 1) The NAA/Cr and Ch/Cr ratios would differ between gray matter and white matter regions, 2) The NAA/Cr ratio would be consistent within gray matter and white matter, but the Ch/Cr ratio would show more regional variability, and 3) Men and women would have similar NAA/Cr and Ch/Cr ratios throughout the brain.

METHODS

Seventy-two healthy subjects (32 men and 40 women) participated in this study. Subjects ranged in age from 22 years old to 44 years. Mean age was 27 years (± 6 years). Subjects were recruited from the university or medical center by word of mouth and email. All subjects had attended college or were in college. Prior to entering the magnet, subjects were provided with a description of the procedure, a consent form to read, and a brief orientation to MR spectroscopy. Subjects filled out a questionnaire regarding past medical and surgical history. All subjects gave written informed consent. Exclusion criteria included claustrophobia, pregnancy, history of serious medical or neurological illness and failure to fulfill the safety criteria developed by the Diagnostic Radiology Department for patients undergoing MRI. The institutional review board approved this study.

Magnetic resonance studies were performed on a GE Signa MRI system (General Electric, Milwaukee, WI) at a magnetic field strength of 1.5 Tesla. Subjects lay supine in the magnet with their heads immobilized by a neck support, foam wedges, and a restraining band drawn around the forehead. Scout images in the sagittal plane were acquired with parameters of 500/11 (TR/TE), a field of view of 24 cm, an imaging matrix of 256 X 192, and 5-mm contiguous sections. Axial T2-weighted images were acquired through the entire brain using a fast spin echo sequence with parameters of 3000/80 (TR/TE), a field of view of 22 cm, an imaging matrix of 256 x 192, an echo train length of 16, and 3 mm contiguous sections. Based on the T2-weighted images, voxels in ten regions of the brain were chosen for MRS spectra (see below). Voxels were 2 x 2 x 2 cm or 2 x 2 x 1.5 cm in size. The spectra were acquired using a point-resolved ^{1}H

spectroscopy (PRESS) technique, which is part of the fully automated Proton Brain Exam-Single Voxel (PROBE-SV) software package supplied by General Electric Medical Systems (GE Medical Systems, Milwaukee, WI). After the transmitter and receiver were automatically adjusted, water signal was automatically shimmed to within a line width of 3-5 Hz. The parameters for MRS were 2000/135 (TR/TE), a field of view of 22 x 22 cm, an imaging matrix of 256 x 192, total number of scans was 128, and scan time was 4 min 56 sec. All data processing was performed by software provided by the manufacturer. Spectral processing included zero-filling, Gaussian apodization, Fourier transformation, water reference processing, frequency shift correction, and phase and baseline correction. Using the curve-fitting software provide by the manufacturer, peak integral values were determined. *N*-acetyl aspartate (NAA) was assigned at 2.02 ppm, choline (Ch) at 3.2 ppm, and creatine (Cr) at 3.03 ppm. The peak areas of NAA, and Ch were normalized with respect to Cr. The integral value of each peak was dimensionless and represented relative measurement of the amount of each metabolite. The ratios NAA/Cr and Ch/Cr were calculated. Spectra and integral values were displayed next to an anatomic T2-weighted image on which a square box was overlaid to indicate the anatomic location of each voxel from which the spectra was obtained.

In the exam time available, all ten brain regions could not be studied in each subject, so spectra from three or four regions were sampled in three different subject groups. In group 1, 22 subjects (10 men, 12 women) had spectra collected from the three brain regions: the occipital lobe gray matter, which included aspects of the cuneus, lingual gyrus and calcarine fissure, the lentiform nuclei (basal ganglia), and the posterior white matter (primarily the parietal lobe). Group 2 consisted of 31 subjects (12 men, 19

women) who had spectra collected from three brain regions: the frontal gray matter (superior frontal gyri), the frontal white matter (bordering superior and middle frontal gyri), and the pons. Fifteen of group 2 subjects also had spectra collected from the temporal gray matter (primary auditory cortex in posterior aspect of the superior temporal gyrus). In group 3, 20 subjects (10 men, 10 women) had spectra collected from three brain regions: the thalamus, the cerebellum (hemisphere), and the parietal gray matter (middle aspect of the intraparietal sulcus). Thirteen of group 3 subjects also had spectra collected from the temporal gray matter as in group 2. Voxels in cerebral gray matter regions were mainly gray matter (approximately 70%), but the inclusion of subcortical white matter could not be avoided. Voxels in cerebral white matter regions were primarily all white matter, with little or no inclusion of gray matter. Voxels in the lentiform nuclei and thalamus contained small amounts of adjacent white matter tracts. The pons consisted of both white matter tracts and brainstem gray matter nuclei. Voxels in the cerebellum consisted of both gray and white matter. The midline, which includes left and right hemispheric tissue, was examined for the frontal gray matter and the occipital gray matter. The left hemisphere was examined for the seven other cerebral and cerebellar regions. For the one brainstem region, the midline of the pons was studied. Figures 1-4 illustrate the ten different brain regions and their corresponding spectra.

An ANOVA with age as the dependent variable and group as a factor demonstrated no significant difference between the mean ages of the three subject groups ($F(2, 64) = .95$, $p = .4$). The mean ages were 29, 27, and 27. An omnibus MANOVA was performed that collapsed across the three groups and examined the two metabolite ratios as the dependent measures and brain region (all ten regions) and gender as independent

variables, or factors. Post-hoc analysis consisted of the Scheffé's F statistic for any significant difference between pairs of brain regions for both the NAA/Cr ratio and the Ch/Cr ratio. To guard against the possibility that significant effects or interactions of brain region and gender could result from differences in variance among the three groups of subjects, a separate multifactorial analysis of variance (MANOVA) was performed for each of the three subject groups with the metabolic ratios of NAA/Cr and Ch/Cr as the dependent variables and with brain region and gender as factors. Post-hoc analysis again consisted of the Scheffé's F statistic for significant differences between pairs of brain regions for both NAA/Cr and Ch/Cr.

RESULTS

The omnibus MANOVA for the NAA/Cr ratio collapsed across the three groups and ten brain regions revealed a main effect of brain region ($F(9,213) = 27$, $p < .0001$), indicating regional variation for the NAA/Cr ratio. There was no main effect of gender ($F(1, 213) = 0.123$, $p = .73$) and no interaction between brain region and gender ($F(9, 213) = .614$, $p = .78$). Table 1 lists the mean NAA/Cr ratio and standard deviation for the ten brain regions, collapsed across gender. The omnibus MANOVA for the Ch/Cr ratio demonstrated a main effect of brain region ($F(9, 213) = 85$, $p < .0001$), again indicating regional variation of Ch/Cr. There was no effect of gender ($F(1, 213) = 1.26$, $p = .26$), and no interaction between brain region and gender ($F(9, 213) = .742$, $p = .67$). Table 2 shows the mean Ch/Cr ratio and standard deviation for the ten brain regions collapsed across gender.

The main effect of brain region and lack of an effect of gender were confirmed with the additional MANOVAs calculated separately for each of the three subject groups. The MANOVA for Group 1 (basal ganglia, occipital gray matter and posterior white matter) for the NAA/Cr ratio demonstrated a main effect of brain region ($F(2, 56) = 30$, $p < .0001$) but no effect of gender ($F(1, 56) = 2.384$, $p = .13$) and no interaction between brain region and gender ($F(2, 56) = 0.87$, $p = .42$). Results for the Ch/Cr ratio demonstrated a main effect of brain region ($F(2, 56) = 74$, $p < .0001$) but no effect of gender ($F(1, 56) = 1.3$, $p = .25$), and no interaction between brain region and gender ($F(2, 56) = .027$, $p = .97$). The separate MANOVA for Group 2 (frontal gray matter, frontal white matter, temporal gray matter and pons) for the NAA/Cr ratio demonstrated a main effect of brain region ($F(3, 90) = 25$, $p < .0001$) but no effect of gender ($F(1, 90) = .109$,

p = .74) and no interaction between brain region and gender (F (3, 90) = 0.165, p = .92). Results for the Ch/Cr ratio demonstrated a main effect of brain region (F (2, 56) = 74, p < .0001) but no effect of gender (F (1, 56) = 1.3, p = .25), and no interaction between brain region and gender (F (2, 56) = .027, p = .97). The separate MANOVA for Group 3 (parietal gray matter, temporal gray matter, thalamus, and cerebellum) for the NAA/Cr ratio demonstrated a main effect of brain region (F (3, 54) = 23, p < .0001) but no effect of gender (F (1, 54) = .002, p = .96) and no interaction between brain region and gender (F (3, 54) = 0.165, p = .25). Results for the Ch/Cr ratio demonstrated a main effect of brain region (F (2, 56) = 74, p < .0001) but no effect of gender (F (1, 56) = 1.3, p = .25), and no interaction between brain region and gender (F (2, 56) = .027, p = .97).

To determine which brain regions differed for a given metabolic ratio, the post-hoc analysis consisted of calculating the Scheffé's F statistic for pair-wise comparisons between brain regions for the NAA/Cr ratio (Table 3) and the Ch/Cr ratio (Table 4), respectively. Forty-five pair-wise comparisons were made for both metabolic ratios. Twenty-one comparisons were significant for the NAA/Cr ratio (Table 3) and twenty-eight comparisons were significant for the Ch/Cr ratio (Table 4). For the NAA/Cr ratio, a direct comparison of regions containing predominately gray matter, like the four cerebral cortical regions and the gray matter nuclei of the basal ganglia and thalamus, did not show significant differences among each other. Similarly, a comparison of regions containing predominately white matter, like the frontal white matter and the posterior white matter, did not differ from each other. The white matter regions also did not differ from the pons. Each cortical gray matter had a smaller ratio than each cerebral white matter region and the pons. Each cortical gray matter region except the frontal area had a

larger ratio than the cerebellum, with the frontal area not showing a significant difference with the cerebellum. The NAA/Cr ratio of the basal ganglia was significantly smaller than the frontal and posterior white matter regions and the pons, but was not significantly different from the cerebellum. The thalamic NAA/Cr ratio, however, did not differ from the cortical white matter regions or the pons, but was larger than the cerebellum.

The Ch/Cr ratio varied widely across different brain regions (Table 2 and Table 4). The cortical gray matter sites showed significant differences between each other, with only the occipital gray and parietal gray matter regions having similar Ch/Cr ratios. The ratio in the occipital gray matter was smaller than the ratio in the frontal and temporal regions. The Ch/Cr ratios in the two cortical white matter sites were equivalent, but unlike the NAA/Cr ratio, they had significantly different (smaller) ratios compared with the pons. The basal ganglia and thalamus had statistically similar Ch/Cr ratios. The basal ganglia showed few significant differences with other regions. The thalamus also differed with only a few regions. The post-hoc analyses for both metabolic ratios resulting from the MANOVA performed separately for each group yielded findings similar to the post-hoc analyses from the omnibus MANOVA.

DISCUSSION

The results reported in this study are generally consistent with those from earlier studies, in terms of regional effects in brain metabolites (21;24;26). In this study, significant differences in NAA/Cr were consistently observed between white matter and gray matter. The regions of white matter had a larger NAA/Cr ratio compared with the smaller ratios of the cortical gray matter, basal ganglia, and cerebellum. Other differences in NAA/Cr ratios were also seen. The pons had a larger ratio than the gray matter, basal ganglia and cerebellum. The cerebellum had a smaller ratio compared to the gray matter and the thalamus. The NAA/Cr ratio did not vary within gray matter or within white matter sites, as there were no significant differences in NAA/Cr when comparing the ratio within gray matter regions and cortical nuclei, or within white matter regions and the pons.

The Ch/Cr ratio demonstrated more regional variability than NAA/Cr, including dissimilarity within gray matter sites (Table 2 and Table 4). Within predominantly white matter sites, however, the Ch/Cr ratio did not differ significantly. The regional variability in choline compounds has been noted previously (26). Other studies looking at regional variations in brain metabolites have found differences between white and gray matter and have even correlated this heterogeneity seen in vivo with in vitro findings, but for the most part this has been done using actual quantification of metabolites (20;26). Most of these studies, even those that used metabolite ratios (5;21), employed different parameters of data acquisition than this study, hindering the ability to make in depth comparisons between this study and previous ones. However, Marshall et al. measured NAA, Ch, Cr, NAA/Ch and NAA/Cr in the right and left parietal white matter of normal

male and female volunteers using similar parameters as our study (PRESS sequence and TE = 135 ms) (27). They reported mean NAA/Cr ratios (measured on consecutive days) of 2.39 ± 0.39 and 2.41 ± 0.50 on right parietal white matter, and 2.55 ± 0.64, 2.34 ± 0.28 on left parietal white matter. These values are consistent with the mean NAA/Cr ratio in posterior white matter observed in our study (2.419 ± 0.266).

The Ch/Cr ratio varied significantly within the gray matter locations compared in our study. This variability could be technical in nature due to data collection and processing limitations or errors. For example, the large voxel size inherent to single voxel MRS means that volumes of interest do not contain only one tissue type. Nevertheless, this variability could still be biological in nature since the same collection and processing parameters were used to calculate NAA/Cr, and no variation was observed in those ratios within gray and white matter sites. Our results, as well as others reported in the literature, could be refined by segmenting gray and white matter to achieve a more homogeneous volume of interest, and by off-line processing of data.

There were no significant effects of gender on either metabolite ratio across all ten regions examined. This finding is consistent with prior studies which used STEAM sequence and short TE in their evaluation of gender differences (21;24;26).

The methodology utilized in the acquisition and processing of data in this study includes the same techniques employed at the clinical MRI center of the Yale University School of Medicine. Some distinguishing features of the data in this study include the use of single voxel PRESS technique employing a relatively large voxel size (6-8 cm3), a long echo time (TE = 135 ms), and metabolite peak area ratio calculations instead of absolute chemical concentrations. Single voxel spectroscopy with automated processing

is widely available for clinical use because it is simple and easy to implement, achieves excellent shim on small volumes, and produces a single spectrum that is immediately accessible for interpretation. In comparison, multivoxel spectroscopy allows acquisition of data from many locations at the same time and improves detection of regional variability, but suffers from reduced SNR and more prominent sensitivity to differences in susceptibility (1).

The voxel size used for spectra acquisition and the number of acquisitions are directly proportional to the SNR. Reducing the voxel size requires an increase in the number of acquisitions, and therefore the scanning time, in order to maintain the same SNR (1). The large voxel size used in this study makes it more difficult to detect small regional differences in spectra, but it allows for a better SNR in a shorter scanning time.

Voxel placement in certain locations, particularly the cerebellum, basal ganglia and the pons in this study, can make it difficult to shim properly. These regions of interest are close to the bones, which interfere with the shimming, affect the spectral quality and therefore, the metabolite ratios obtained. Additional shimming procedures, off-line processing and segmentation of gray and white matter improve ratio quantification of metabolites, but clinical interpretation of spectra rarely uses these additional corrections.

Longer echo times, like the TE of 135 ms used in this study, offer the benefit of a simpler spectrum with less peak interference from lipid signals, which facilitates the interpretation of the spectrum. However, long TE MRS is less sensitive to metabolites with short T2 whose variations may be important to the diagnosis of certain diseases. PRESS localization is the sequence of choice for long TE spectroscopy because it

provides a higher SNR and a lower sensitivity to motion compared to STEAM sequences (1).

Quantification of metabolites in MRS can be difficult, so a more practical and easier way to assess variations in metabolite levels is by calculating peak area ratios. Metabolite ratios, like those calculated in this study using Cr as a reference, are favored for clinical MRS because they are simple to obtain, require no technical expertise or additional software, are not dependent on changes in coil loading or other differences among individuals, and do not require relaxation-time measurements. Also, ratios are unaffected by cerebral spinal fluid contamination because the metabolites of interest are much lower in the CSF. The disadvantage of using metabolic ratios is that they are sensitive to changes in the concentration of both metabolites in the ratio. Using Cr as a reference in our study assumes that its concentration does not change; however, this is not always the case. Interpretation of NAA and Ch relative to Cr could result in a misleading ratio.

Ideally, metabolite measurement of all ten regions of interest in our study would have been obtained in each subject to facilitate the comparison of ratios across the brain locations. Since only three or four regions were measured for each subject group in our study, the main effect of brain region on the metabolic ratio could result from a difference in variance between groups rather than a true difference between brain regions. To account for this possibility, the Scheffé's F statistic, the most conservative of the paired comparison procedures, was used in the data analysis (28). This procedure is useful for post-hoc comparisons if samples sizes vary in size and if there is a possibility of heterogeneous variances among groups. The post-hoc analyses resulted in similar

findings in both the omnibus MANOVA and in the MANOVA calculated separately for each group, suggesting that the three groups of subjects had relatively homogeneous variance with regard to MRS measurements of the metabolic ratios.

Most databases of normal brain metabolites and ratios published to date use short TE proton MRS. There is a need for a normative database based on single voxel MRS acquired with a long TE. The database established in this study utilized such parameters, and will be employed at our institution as a control in the clinical evaluation of patients with proton MRS. The clinical applications of single voxel ^{1}H MRS range from the detection and pre-operative evaluation of epileptic foci and the pre-operative evaluation and post-treatment follow-up of tumors, to the detection of metabolic disorders, especially inborn errors of metabolism and the evaluation of lesion load in multiple sclerosis. Figures 5 and 6 illustrate examples of three clinical cases studied using MRS, including abnormal spectra acquired from a metastasis in the frontal lobe and an astrocytoma in the basal ganglia (Fig. 5), and an abnormal spectrum from a patient with a metabolic disorder resulting in excess glycine (Fig. 6).

The effect of age was not evaluated in this study due to the small number of younger children and older adults that have been studied thus far. The potential age-dependent changes in metabolic ratios should be explored in future studies. Expanding the age range of the current database would be beneficial to the clinical application of MRS at our institution.

REFERENCES

1. Salibi, N., Brown, M.A. 1998. Clinical MR Spectroscopy. New York:Wiley-Liss. 220 pp.

2. Kwock, L. 1998. Localized MR spectroscopy: basic principles. *Neuroimaging Clinics of North America* 8:713-731.

3. Castillo, M., Kwock, L., and Mukherji, S.K. 1996. Clinical applications of proton MR spectroscopy. *Ajnr: American Journal of Neuroradiology* 17:1-15.

4. Kreis, R. 1997. Quantitative localized 1H MR spectroscopy for clinical use. *Journal of Progress in Nuclear Magnetic Resonance spectroscopy* 31:155-195.

5. Grachev, I.D. and Apkarian, A.V. 2000. Chemical heterogeneity of the living human brain: a proton MR spectroscopy study on the effects of sex, age, and brain region. *Neuroimage* 11:554-563.

6. Duncan, J.S. 1996. Magnetic resonance spectroscopy. *Epilepsia* 37:598-605.

7. Kreis, R., Ernst, T., and Ross, B.D. 1993. Development of the human brain: in vivo quantification of metabolite and water content with proton magnetic resonance spectroscopy. *Magnetic Resonance in Medicine* 30:424-437.

8. Peden, C.J., Cowan, F.M., Bryant, D.J., Sargentoni, J., Cox, I.J., *et al.* 1990. Proton MR spectroscopy of the brain in infants. *Journal of Computer Assisted Tomography* 14:886-894.

9. Pouwels, P.J.W., Brockmann, K., Kruse, B., Wilken, B., Wick, M., *et al*. 1999. Regional age dependence of human brain metabolites from infancy to adulthood as detected by quantitative localized proton MRS. *Pediatric Research* 46:474-485.

10. Wang, Z.J. and Zimmerman, R.A. 1998. Proton MR spectroscopy of pediatric brain metabolic disorders. *Neuroimaging Clinics of North America* 8:781-807.

11. Ross, B. and Bluml, S. 2001. Magnetic resonance spectroscopy of the human brain. *Anatomical Record* 265:54-84.

12. Ross, B.D., Bluml, S., Cowan, R., Danielsen, E., Farrow,N., *et al*. 1998. In vivo MR spectroscopy of human dementia. *Neuroimaging Clinics of North America* 8:809-822.

13. Castillo, M. and Kwock, L. 1998. Proton MR spectroscopy of common brain tumors. *Neuroimaging Clinics of North America* 8:733-752.

14. Ricci, P.E., Jr. 1998. Proton MR spectroscopy in ischemic stroke and other vascular disorders. *Neuroimaging Clinics of North America* 8:881-900.

15. Cecil, K.M. and Lenkinski, R.E. 1998. Proton MR spectroscopy in inflammatory and infectious brain disorders. *Neuroimaging Clinics of North America* 8:863-880.

16. Suwanwelaa, N., Phanuphak, P., Phanthumchinda, K., Suwanwela, N.C., Tantivatana, J., *et al*. 2000. Magnetic resonance spectroscopy of the brain in neurologically asymptomatic HIV-infected patients. *Magnetic Resonance Imaging* 18:859-865.

17. Laxer, K.D. 1997. Clinical applications of magnetic resonance spectroscopy. *Epilepsia* 38:S13-17.

18. Hanefeld, F., Holzbach, U., Kruse, B., Wilichowski, E., Christen, H.J., *et al*. 1993. Diffuse white matter disease in three children: an encephalopathy with unique features on magnetic resonance imaging and proton magnetic resonance spectroscopy. *Neuropediatrics* 24:244-248.

19. Michaelis, T., Merboldt, K.D., Bruhn, H., Hanicke, W., and Frahm, J. 1993. Absolute concentrations of metabolites in the adult human brain in vivo: quantification of localized proton MR spectra. *Radiology* 187:219-227.

20. Kreis, R., Ernst, T., and Ross, B.D. 1993. Absolute Quantitation of Water and Metabolites in the Human Brain. II. Metabolite Concentrations. *Journal of Magnetic Resonance, series B* 102:9-19.

21. Komoroski, R.A., Heimberg, C., Cardwell, D., and Karson, C.N. 1999. Effects of gender and region on proton MRS of normal human brain. *Magnetic Resonance Imaging* 17:427-433.

22. Cady, E.B., Penrice, J., Amess, P.N., Lorek, A., Wylezinska, M., *et al*. 1996. Lactate, N-acetylaspartate, choline and creatine concentrations, and spin-spin relaxation in thalamic and occipito-parietal regions of developing human brain. *Magnetic Resonance in Medicine* 36:878-886.

23. Ross, B. and Michaelis, T. 1994. Clinical applications of magnetic resonance spectroscopy. *Magnetic Resonance Quarterly* 10:191-247.

24. Charles, H.C., Lazeyras, F., Krishnan, K.R., Boyko, O.B., Patterson, L.J., *et al*. 1994. Proton spectroscopy of human brain: effects of age and sex. *Progress in Neuro-Psychopharmacology & Biological Psychiatry* 18:995-1004.

25. Wilkinson, I.D., Paley, M.N., Miszkiel, K.A., Hall-Craggs, M.A., Kendall, B.E., *et al*. 1997. Cerebral volumes and spectroscopic proton metabolites on MR: is sex important? *Magnetic Resonance Imaging* 15:243-248.

26. Pouwels, P.J. and Frahm, J. 1998. Regional metabolite concentrations in human brain as determined by quantitative localized proton MRS. *Magnetic Resonance in Medicine* 39:53-60.

27. Marshall, I., Wardlaw, J., Cannon, J., Slattery, J., and Sellar, R.J. 1996. Reproducibility of metabolite peak areas in the 1H MRS of Brain. *Magnetic Resonance Imaging* 14:281-292.

28. Scheffé, H. 1953. A method for judging all contrasts in the analysis of variance. *Biometrika* 40:87-104.

FIGURES AND LEGENDS

Figure 1. Single voxel PRESS proton MR spectra (TR/TE = 2000/135) from cerebral gray matter locations, showing the choline (Ch), creatine (Cr), and N-acetyl aspartate (NAA) peaks. Spin-echo MRI scans in the axial plane, used as an anatomic reference, show the voxel location (left) of the acquired spectra (right). Locations include (A) the frontal lobe of a male subject (voxel size = 2 x 2 x 2 cm); (B) the occipital lobe of a female subject (voxel size = 2 x 2 x 1.5 cm); (C) the parietal lobe of a female subject (voxel size = 2 x 2 x 1.5 cm); and (D) the temporal lobe of a female subject (voxel size = 2 x 2 x 1.5 cm). The chemical shift scale is in parts per million (ppm) relative to tetramethylsilane.

Figure 2. Single voxel PRESS proton MR spectra (TR/TE = 2000/135) from cerebral white matter locations, showing the choline (Ch), creatine (Cr), and N-acetyl aspartate (NAA) peaks. Spin-echo MRI scans in the axial plane shows the voxel locations (left) for the acquired spectra (right). Locations include (A) the frontal lobe white matter of a female subject (voxel size = 2 x 2 x 1.5 cm); and the posterior white matter of a male subject (voxel size = 2 x 2 x 2 cm). The chemical shift scale is in parts per million (ppm) relative to tetramethylsilane.

Figure 3. Single voxel PRESS proton MR spectra (TR/TE = 2000/135), from (A) the basal ganglia (voxel size = 2 x 2 x 2 cm) and (B) the thalamus (voxel size = 2 x 2 x 1.5 cm) of two female subjects, showing the choline (Ch), creatine (Cr), and N-acetyl aspartate (NAA) peaks. A spin-echo MRI scan in the axial plane shows the voxel location

(left) for the acquired spectrum (right). The chemical shift scale is in parts per million (ppm) relative to tetramethylsilane.

Figure 4. Single voxel PRESS proton MR spectrum (TR/TE = 2000/135, voxel size = 2 x 2 x 1.5 cm) from (A) the pons and (B) cerebellum of two female subjects, showing the choline (Ch), creatine (Cr), and N-acetyl aspartate (NAA) peaks. A spin-echo MRI scan in the axial plane shows the voxel location (left) for the acquired spectrum (right). The chemical shift scale is in parts per million (ppm) relative to tetramethylsilane.

Figure 5. Spin-echo MRI of the brain in the axial plane showing a frontal lobe metastatic tumor (A) in a 59 year old female (left), and the corresponding MR spectrum (voxel size = 2 x 2x 1.5 cm, right) showing a decreased NAA peak, and increased lipid signal. Another example of the clinical use of MRS shows a basal ganglia astrocytoma (B) in the axial plane (left), and an abnormal MR spectrum (TE = 135 ms, voxel size = 2 x 2 x 1.5 cm) with a decreased NAA peak, and an elevated Ch peak (right). The chemical shift scale is in parts per million (ppm) relative to tetramethylsilane.

Figure 6. Single voxel PRESS proton MRS (TR/TE = 2000/135) showing normal peaks for Ch, Cr and NAA (left), compared to the spectrum of a patient with non-ketotic hyperglycinemia (right). An elevated glycine peak can be seen at a chemical shift of 3.56 ppm, to the left of the Ch peak. The chemical shift scale is in parts per million (ppm) relative to tetramethylsilane.

Figure 1A

Frontal Gray Matter

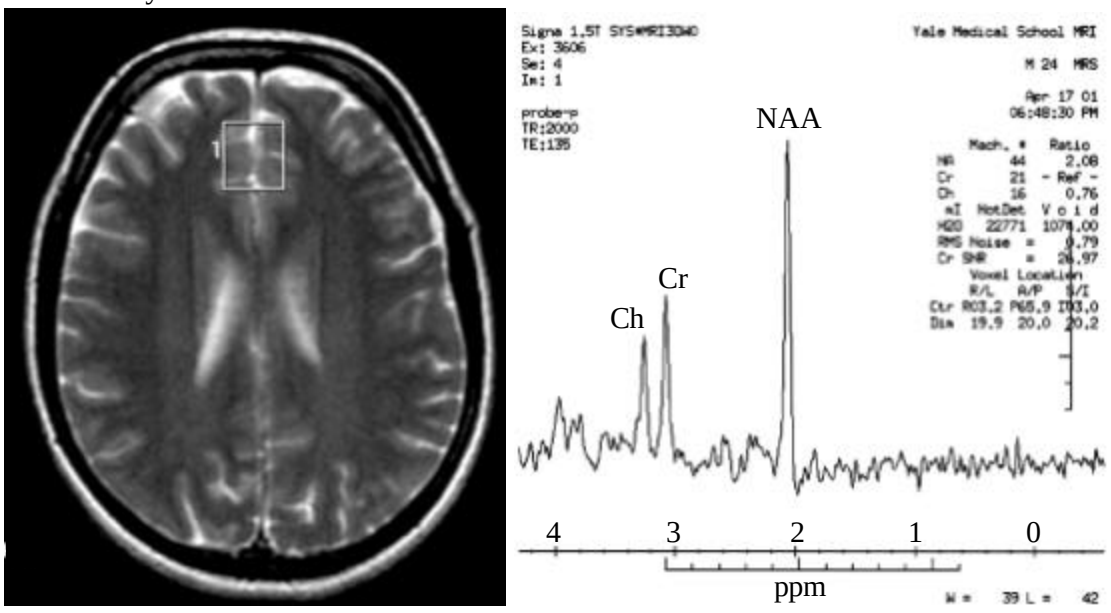

Figure 1B

Occipital Gray Matter

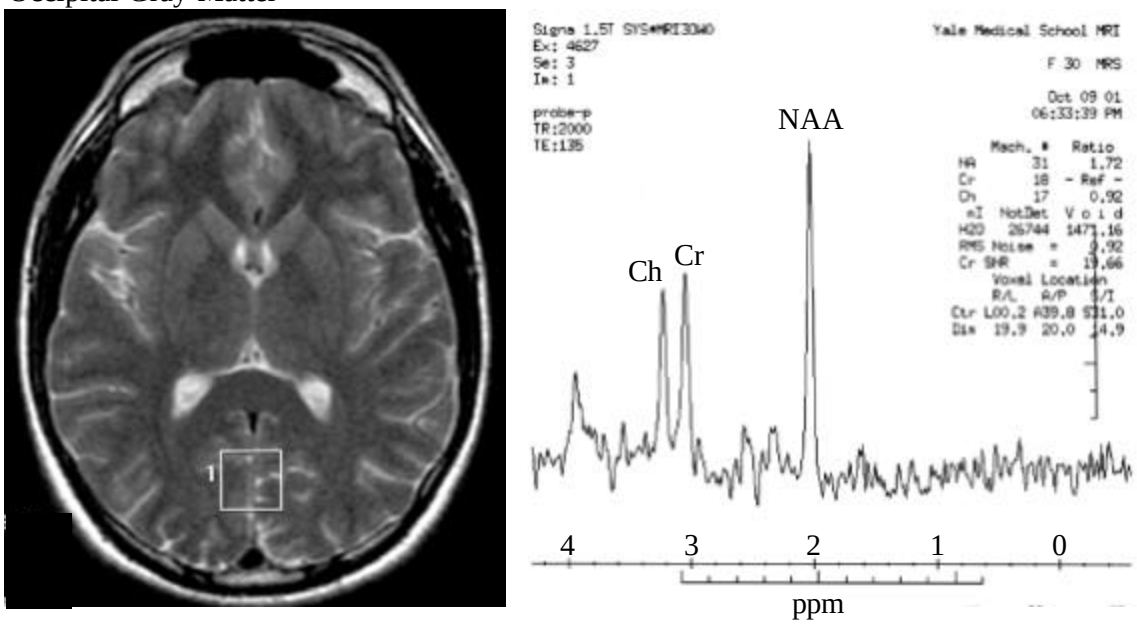

Figure 1C

Parietal Gray Matter

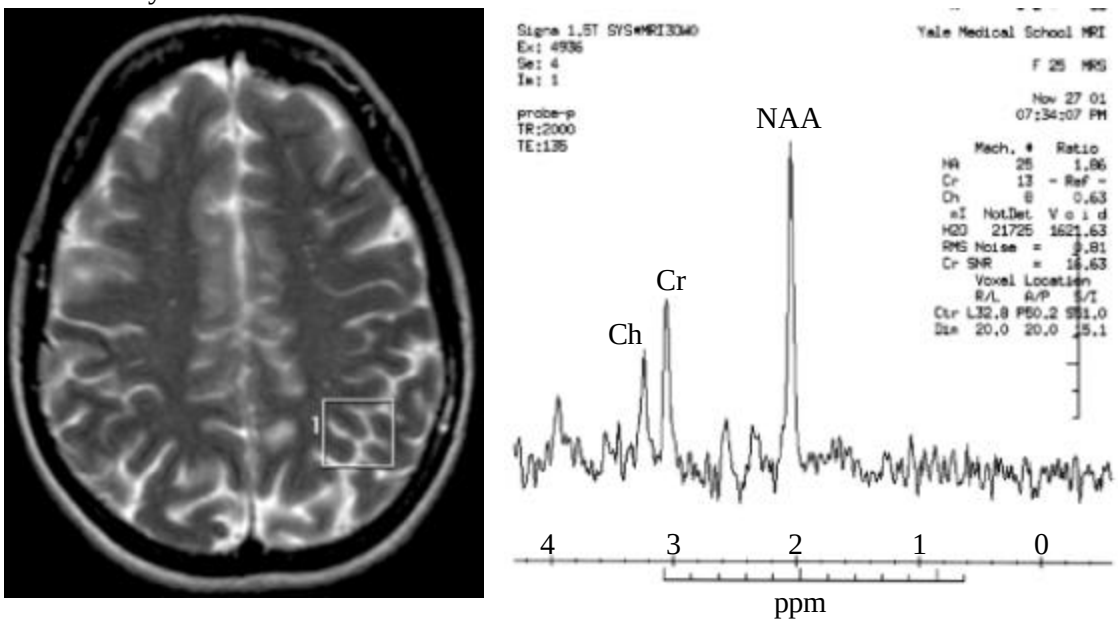

Figure 1D

Temporal Gray Matter

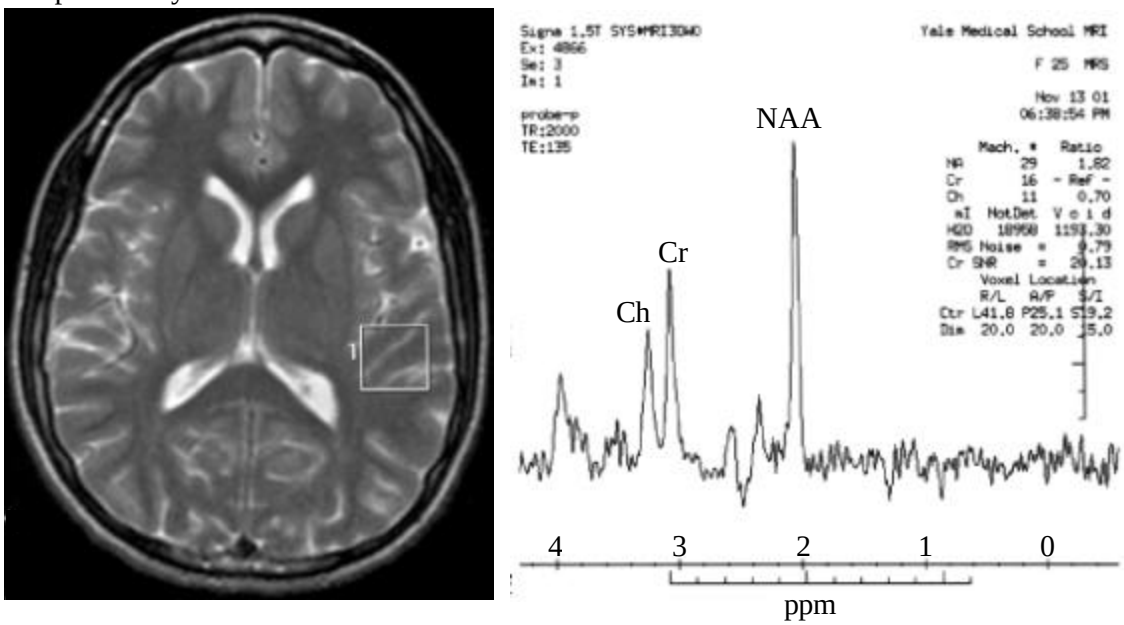

Figure 2A

Frontal White Matter

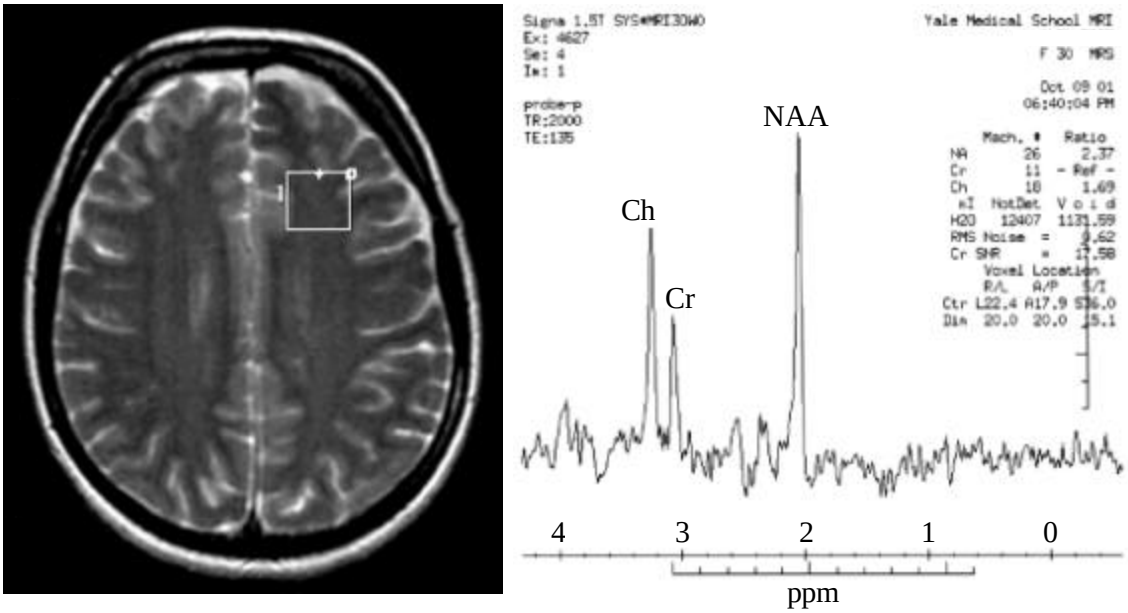

Figure 2B

Posterior White Matter

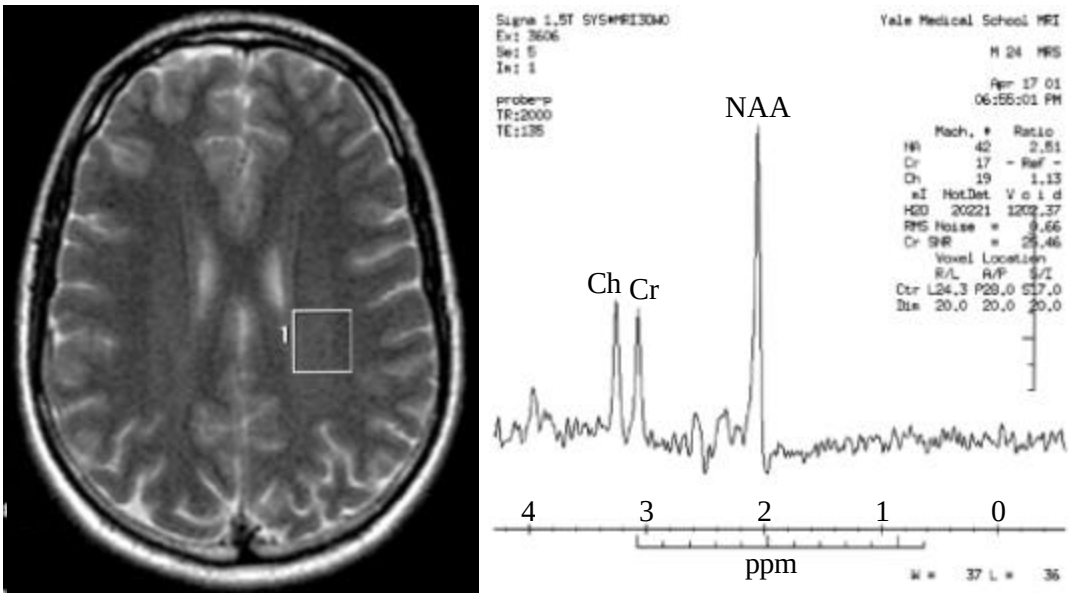

Figure 3A

Basal Ganglia

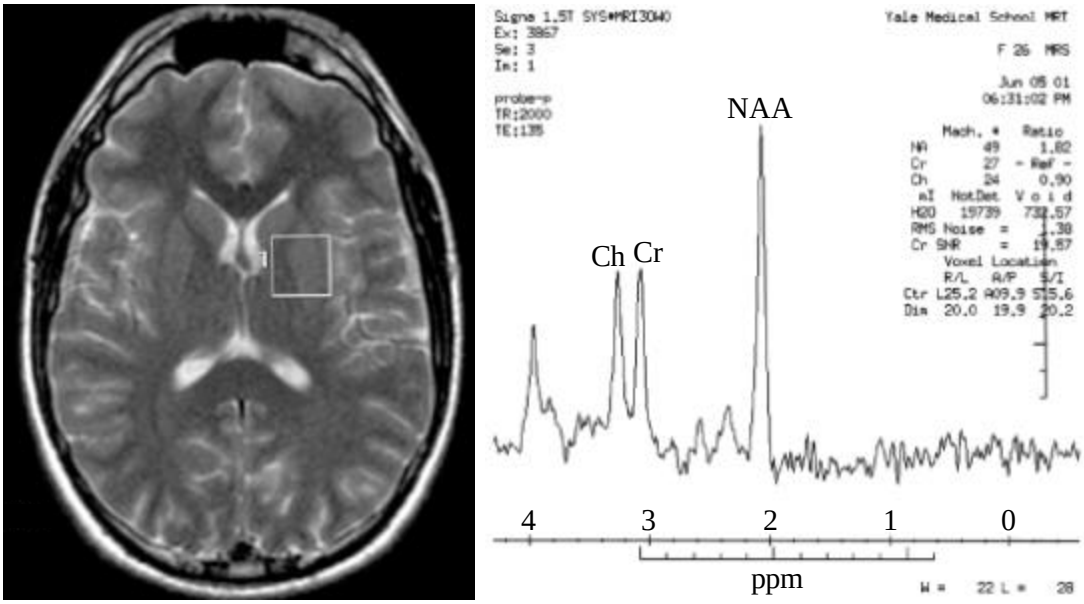

Figure 3B

Thalamus

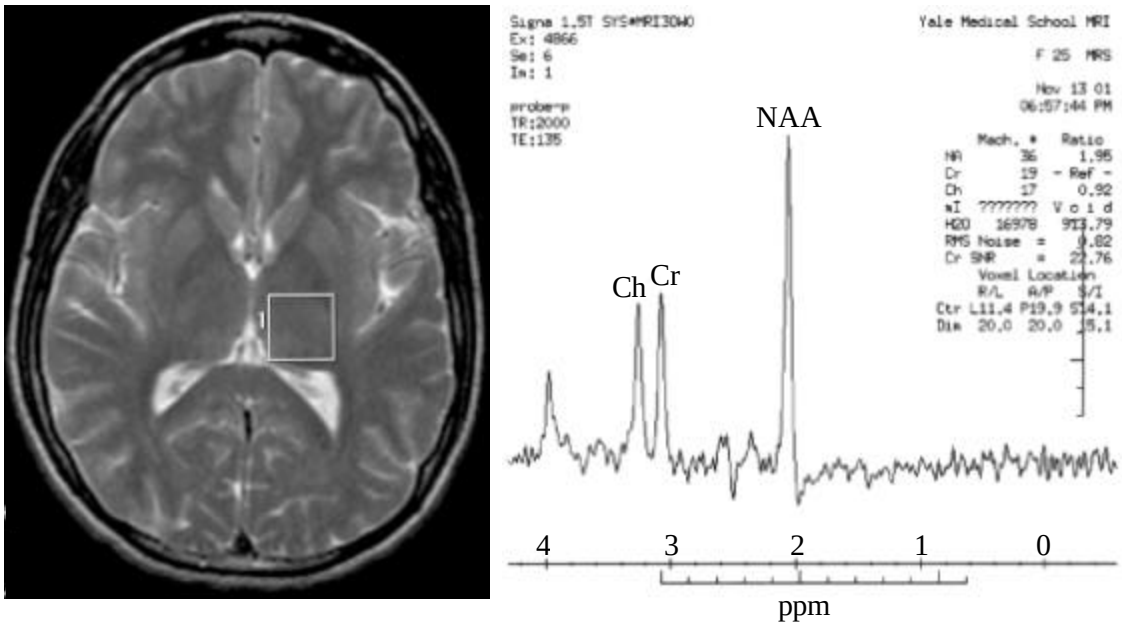

Figure 4A

Pons

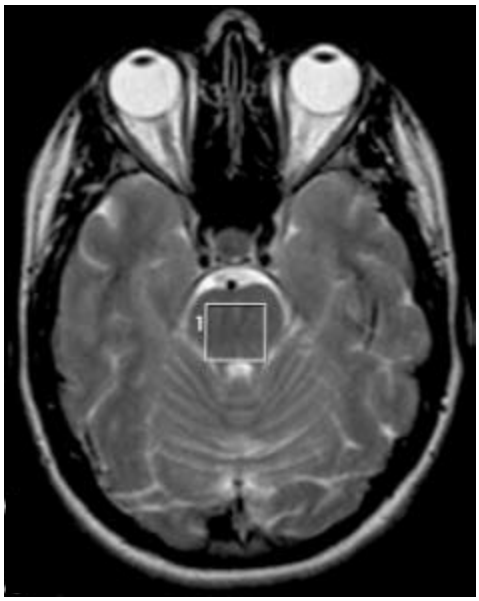

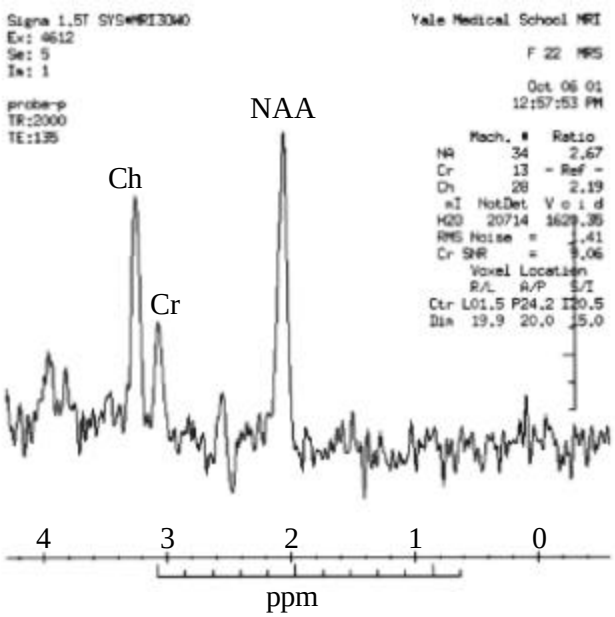

Figure 4B

Cerebellum

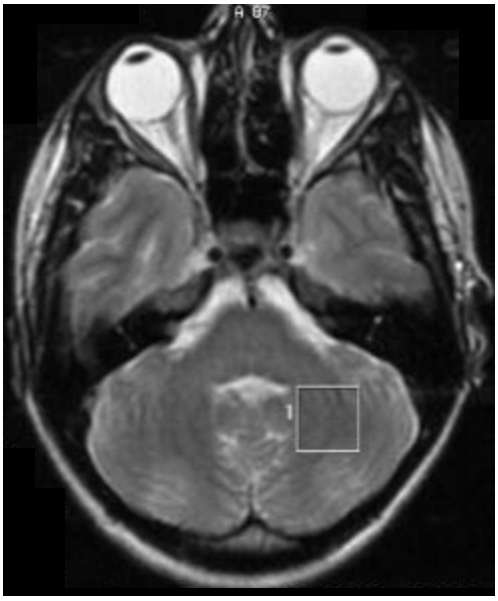

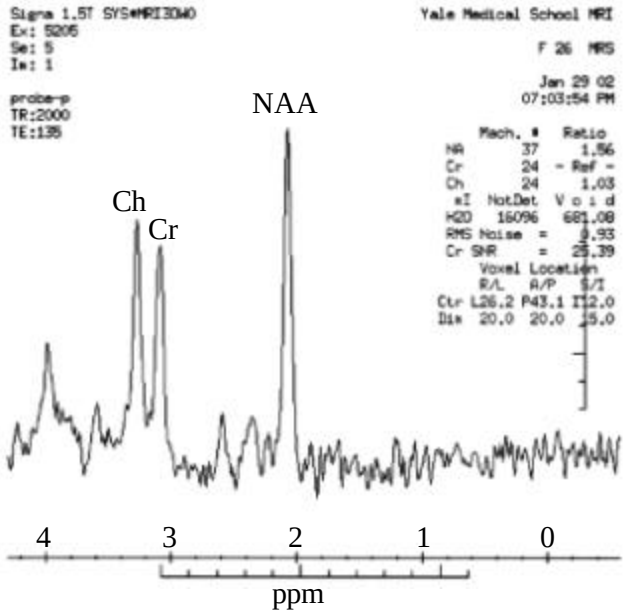

Figure 5A

Frontal lobe tumor

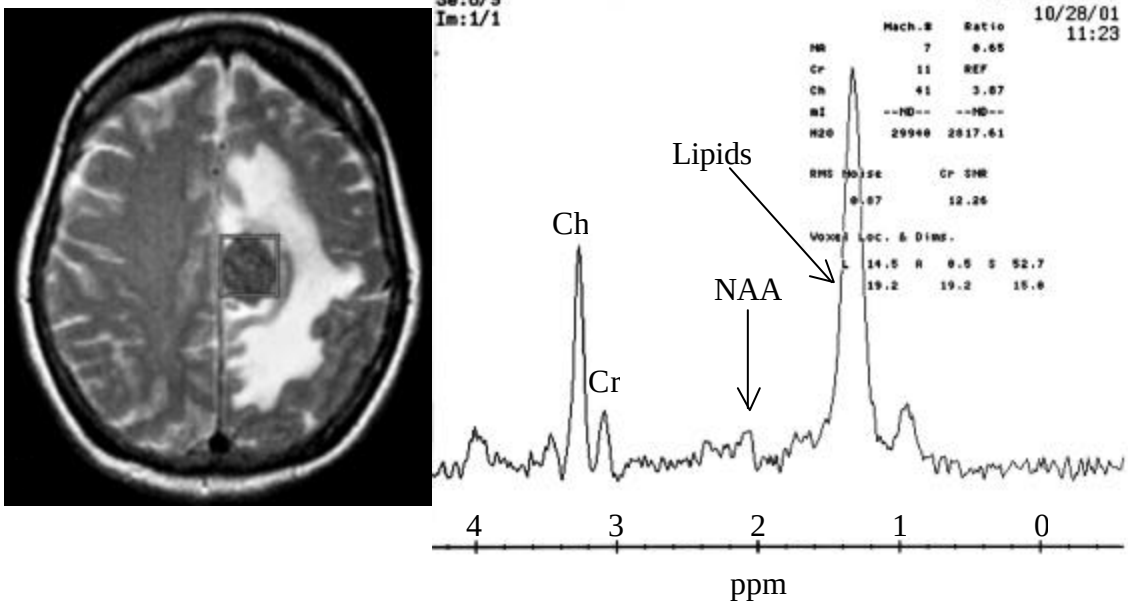

Figure 5B

Basal Ganglia Tumor

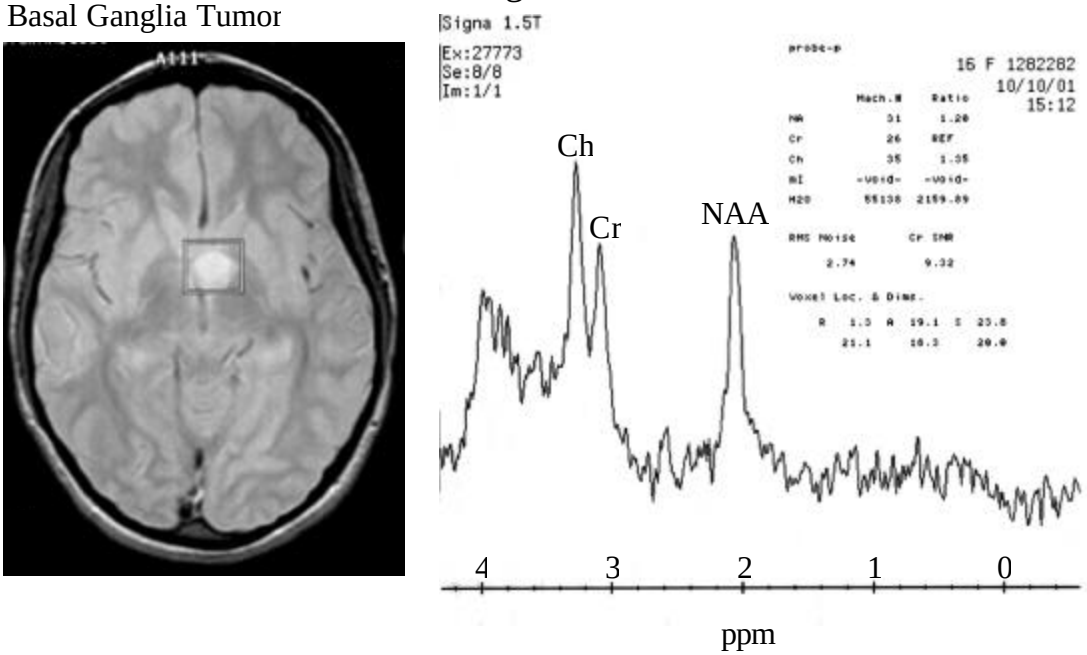

Figure 6

Normal MRS

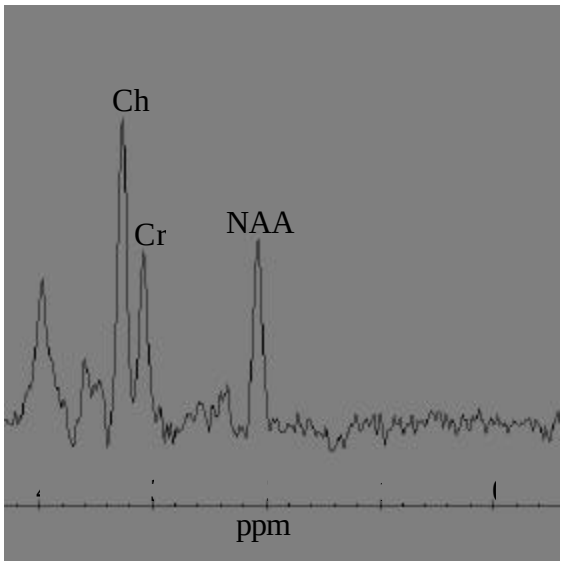

Patient with elevated glycine

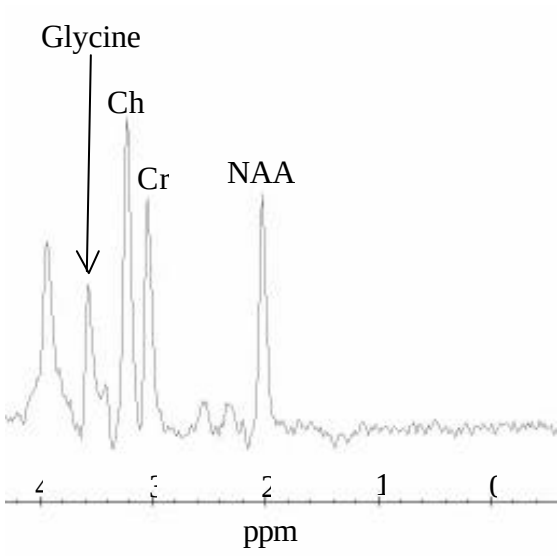

Table 1

Mean NAA/Cr Ratio in 10 Brain Regions

	Count	Mea	Std. Dev.	Std. Err.
bg	20	1.834	.336	.075
occgm	22	2.000	.097	.021
powm	20	2.419	.266	.059
fgm	29	1.789	.210	.039
fwm	27	2.346	.370	.071
pgm	19	2.040	.199	.046
tgm	29	2.026	.192	.036
pons	28	2.427	.364	.069
Th	19	2.093	.228	.052
cb	20	1.512	.262	.059

bg = basal ganglia; occgm = occipital gray matter; powm = posterior white matter; fgm = frontal gray matter; fwm = frontal white matter; pgm = parietal gray matter; tgm = temporal gray matter; Th = thalamus; cb = cerebellum

Table 2

Mean Ch/Cr Ratio in 10 Brain Regions

	Count	Mea	Std. Dev.	Std. Err.
bg	20	1.018	.192	.043
occgm	22	.678	.075	.016
powm	20	1.242	.160	.036
fgm	29	1.144	.156	.029
fwm	27	1.459	.258	.050
pgm	19	.826	.125	.029
tgm	29	.929	.113	.021
pons	28	1.914	.302	.057
Th	19	1.133	.171	.039
cb	20	1.151	.144	.032

bg = basal ganglia; occgm = occipital gray matter; powm = posterior white matter; fgm = frontal gray matter; fwm = frontal white matter; pgm = parietal gray matter; tgm = temporal gray matter; Th = thalamus; cb = cerebellum

Table 3

Scheffe for NAA/Cr
Effect: Brain Region
Significance Level: 5 %

	Mean Diff.	Crit. Diff.	P-Value	
bg, occgm	-.167	.348	.9105	
bg, powm	-.585	.356	<.0001	S
bg, fgm	.044	.327	>.9999	
bg, fwm	-.512	.332	<.0001	S
bg, pgm	-.206	.361	.7707	
bg, tgm	-.192	.327	.7407	
bg, pons	-.593	.330	<.0001	S
bg, Th	-.260	.361	.4441	
bg, cb	.321	.356	.1281	
occgm, powm	-.418	.348	.0043	S
occgm, fgm	.211	.318	.5748	
occgm, fwm	-.345	.324	.0239	S
occgm, pgm	-.040	.353	>.9999	
occgm, tgm	-.025	.318	>.9999	
occgm, pons	-.426	.321	.0006	S
occgm, Th	-.093	.353	.9988	
occgm, cb	.488	.348	.0002	S
powm, fgm	.629	.327	<.0001	S
powm, fwm	.073	.332	.9997	
powm, pgm	.379	.361	.0294	S
powm, tgm	.393	.327	.0044	S
powm, pons	-.008	.330	>.9999	
powm, Th	.325	.361	.1277	
powm, cb	.906	.356	<.0001	S
fgm, fwm	-.556	.301	<.0001	S
fgm, pgm	-.251	.332	.3684	
fgm, tgm	-.237	.296	.2776	
fgm, pons	-.637	.298	<.0001	S
fgm, Th	-.304	.332	.1146	
fgm, cb	.277	.327	.2007	
fwm, pgm	.306	.337	.1230	
fwm, tgm	.320	.301	.0255	S
fwm, pons	-.081	.304	.9986	
fwm, Th	.252	.337	.3807	
fwm, cb	.833	.332	<.0001	S
pgm, tgm	.014	.332	>.9999	
pgm, pons	-.387	.335	.0080	S
pgm, Th	-.053	.365	>.9999	
pgm, cb	.528	.361	<.0001	S
tgm, pons	-.401	.298	.0005	S
tgm, Th	-.067	.332	.9999	
tgm, cb	.513	.327	<.0001	S
pons, Th	.334	.335	.0518	
pons, cb	.914	.330	<.0001	S
Th, cb	.581	.361	<.0001	S

bg = basal ganglia; occgm = occipital gray matter; powm = posterior white matter; fgm = frontal gray matter; fwm = frontal white matter; pgm = parietal gray matter; tgm = temporal gray matter; Th = thalamus; cb = cerebellum; S = significant

Table 4

Scheffe for Ch/Cr Ratio
Effect: Brain
Significance Level: 5 %

	Mean Diff.	Crit. Diff.	P-	
bg, occgm	.340	.241	.0002	S
bg, powm	-.224	.246	.1199	
bg, fgm	-.126	.227	.7992	
bg, fwm	-.441	.230	<.0001	S
bg, pgm	.192	.250	.3400	
bg, tgm	.089	.227	.9743	
bg, pons	-.896	.228	<.0001	S
bg, Th	-.115	.250	.9313	
bg, cb	-.133	.246	.8253	
occgm, powm	-.564	.241	<.0001	S
occgm, fgm	-.466	.220	<.0001	S
occgm, fwm	-.781	.224	<.0001	S
occgm, pgm	-.149	.244	.6968	
occgm, tgm	-.251	.220	.0099	S
occgm, pons	-1.236	.222	<.0001	S
occgm, Th	-.455	.244	<.0001	S
occgm, cb	-.474	.241	<.0001	S
powm, fgm	.098	.227	.9531	
powm, fwm	-.217	.230	.0878	
powm, pgm	.416	.250	<.0001	S
powm, tgm	.313	.227	.0003	S
powm, pons	-.672	.228	<.0001	S
powm, Th	.109	.250	.9488	
powm, cb	.091	.246	.9844	
fgm, fwm	-.315	.208	<.0001	S
fgm, pgm	.318	.230	.0003	S
fgm, tgm	.216	.205	.0281	S
fgm, pons	-.770	.207	<.0001	S
fgm, Th	.012	.230	>.9999	
fgm, cb	-.007	.227	>.9999	
fwm, pgm	.633	.233	<.0001	S
fwm, tgm	.530	.208	<.0001	S
fwm, pons	-.455	.210	<.0001	S
fwm, Th	.326	.233	.0002	S
fwm, cb	.307	.230	.0006	S
pgm, tgm	-.102	.230	.9436	
pgm, pons	-1.088	.232	<.0001	S
pgm, Th	-.306	.253	.0037	S
pgm, cb	-.325	.250	.0010	S
tgm, pons	-.985	.207	<.0001	S
tgm, Th	-.204	.230	.1447	
tgm, cb	-.223	.227	.0591	
pons, Th	.781	.232	<.0001	S
pons, cb	.762	.228	<.0001	S
Th, cb	-.019	.250	>.9999	

bg = basal ganglia; occgm = occipital gray matter; powm = posterior white matter; fgm = frontal gray matter; fwm = frontal white matter; pgm = parietal gray matter; tgm = temporal gray matter; Th = thalamus; cb = cerebellum; S = significant